JOURNAL OF EXPERIMENTAL AND THEORETICAL PHYSICS, 2024, Vol. 165, No. 5, pp. 613–623

ATOMS, MOLECULES, OPTICS

INTERFERENCE EFFECTS OF DIFFERENT CHANNELS OF PULSED EXCITATION OF COHERENT POPULATION TRAPPING RESONANCES IN CELLS WITH ALKALI METAL VAPORS AND BUFFER GAS

© 2024 G. V. Voloshin *, K. A. Barantsev, A. N. Litvinov

Peter the Great St. Petersburg Polytechnic University, 195251, St. Petersburg, Russia

** e-mail: gavriilvsh@gmail.com*

Received September 28, 2023

Revised November 17, 2023

Accepted November 17, 2023

Abstract. A theory of Ramsey resonance excitation has been developed, taking into account the complete magnetic structure of levels D_1-line of ^{87}Rb atoms, as well as the finite temperature of the ensemble. The dependences of the shape and shifts of resonances on parameters such as external magnetic field magnitude, degree of laser field ellipticity, and medium temperature have been analyzed. The possibility of interference between different channels of Ramsey resonance excitation, observed when varying the magnetic field magnitude, is shown. The existence of optimal field ellipticity at certain polarization, leading to the highest resonance amplitude, has also been discovered.

DOI: 10.31857/S004445102405e018

1. INTRODUCTION

The phenomenon of coherent population trapping (CPT) represents the emergence of such a superposition quantum state that does not interact with laser radiation. This situation can be realized through the interaction of bichromatic laser radiation with atomic ensembles [1-4]. In the absorption spectrum, this manifests as the emergence of a transparency window, which can be hundreds or even tens of hertz wide. The presence of a narrow resonance allows the use of the CPT phenomenon in various practical applications: optical magnetometry [5-8], lasing without inversion [9], quantum informatics [10-12], compact frequency standards [13-20].

One of the most important tasks of high-precision spectroscopy is obtaining narrow and highcontrast CPT resonances. The use of continuous pumping of laser sources imposes certain limitations on the resonance width. At the same time, a significant narrowing of the CPT resonance line can be achieved by implementing pulsed pumping or the Ramsey scheme [21]. The essence of this method lies in the interaction of an atomic ensemble with two consecutive pulses (pumping and reading), separated by a dark pause [22]. As a result, the width of the CPT resonance is determined only by the dark pause, which allows achieving a significantly narrower CPT resonance line [22].

Currently, active research is being conducted on two-photon resonances (coherent population trapping and double radio-optical resonance (DROR)) using pulsed pumping. The authors of work [23] described a method for stabilizing the amplitude of the interrogating microwave field in compact atomic clocks based on DROR using the Ramsey interrogation scheme. In work [24], it was shown that Raman-Ramsey interference is a highly effective method for implementing compact and high-performance frequency standards based on CPT in buffer gas cells. In this work, the authors theoretically investigated Raman-Ramsey resonances in optically dense atomic vapors. The emergence of Ramsey comb shifts and "clipping" of its maxima in the Ramsey interrogation scheme of CPT resonance in a cold dilute atomic ensemble in an optically dense medium is shown in [25]. Experimental study of CPT resonances based on the Raman-Ramsey technique in cells containing gas mixture ^{87}Rb–Ar–Ne for lin *lin* $\parallel$ *lin* configuration was conducted in [26], and for cells with atoms ^{133}Cs — in

[27]. The influence of hyperfine structure on the CPT resonance shape in the Ramsey interrogation scheme in cold and hot atoms is analyzed in works [28, 29]. A consistent theory of bichromatic laser radiation interaction with an optically dense medium of alkali atoms having non-zero temperature under pulsed pumping is presented in [30]. Methods for suppressing light shifts of CPT resonances under pulsed pumping based on the auto-balanced scheme were experimentally investigated in [31]. The auto-balanced scheme in an optically dense medium is theoretically considered in [32]. The possibility of suppressing field shifts of CPT resonance using methods of generalized auto-balanced Ramsey spectroscopy and combined error signal is demonstrated in [33]. The authors of work [34] succeeded in implementing a rubidium quantum frequency standard based on DROR, using pulsed pumping and achieving stability $2.5 \cdot 10^{-13}$ per second. The results of work [35] showed that this is not the limit. The authors of this work managed to improve the previous result and achieve atomic clock stability, also based on DROR and using pulsed optical pumping of "hot" atoms, to values of $1.2 \cdot 10^{-13}$ per second [35]. Work [36] emphasizes that multi-pulse CPT-Ramsey interferometry is a powerful tool for improving the characteristics of CPT-based atomic clocks. The authors analyzed multi-pulse CPT-Ramsey interferometry for arbitrary pulse sequences and obtained a generalized analytical expression.

Summarizing, we can see that the study of CPT resonances under pulsed pumping is a relevant direction. Currently, theoretical research in this direction has allowed developing the theory of laser pulse radiation interaction under CPT resonance conditions in "hot" atoms in the absence of degeneracy between hyperfine levels in optically thin [29,36] and optically dense [24, 25, 28, 30] media. The theory of CPT resonances in alkali metal vapors in cells with buffer gas, considering the "real" structure of energy levels and polarization of light waves for continuous excitation by a two-frequency field [37], has been constructed quite comprehensively. However, there is no similar theory of CPT resonance for pulsed pumping. The aim of this work is to fill this gap and describe the interaction of laser radiation with alkali atoms at room (and higher) temperatures. Simultaneously, we assume that laser radiation has arbitrary polarization, and active atoms are in an external magnetic field, which leads to the removal of degeneracy between Zeeman sublevels.

2. MATHEMATICAL MODEL

Let's consider a medium of atoms ^{87}Rb in the field of bichromatic laser radiation, quasiresonant to the D_1-line of atoms (see Fig. 1). The external electric field strength vector can be written as

$$\mathbf{E}(\mathbf{r},t) = \mathbf{E}_1(\mathbf{r},t)\exp- i(\omega_1 t - k_1 z) + \\ + \mathbf{E}_2(\mathbf{r},t)\exp- i(\omega_2 t - k_2 z) + \text{c.c.}, \quad (1)$$

where ω_j, k_j — frequencies and wave vectors of the corresponding frequency components of the wave ($j = 1,2$). Here

$$\mathbf{E}_j(\mathbf{r},t) = E_j(\mathrm{r},t)\mathrm{e}_j = E_j(\mathrm{r},t)(p_j^+ \mathrm{e}_+ + p_j^- \mathrm{e}_-) \quad (2)$$

— complex amplitudes of the frequency components of the electric field strength, decomposed into covariant cyclic unit vectors

$$\mathrm{e}_\pm = \mathrm{e}^{\pm *} = \mp(\mathrm{e}_x \pm i\mathrm{e}_y) / \sqrt{2}$$

with coefficients $p_j^\pm$. The values of these coefficients determine the polarization state of radiation. Note that these amplitudes are related to intensities I_j as

$$| \mathbf{E}_j | = \sqrt{2\pi I_j / c}.$$

Further, we will use the optical thinness approximation of the medium, neglecting the coordinate dependencies of these amplitudes. We will also neglect the possibility of incoherent scattering associated with radiation reabsorption in the medium [38-41].

The quantum state of the atomic ensemble will be described through the single-particle Wigner density matrix $\hat{\rho}(\mathrm{r}, \mathrm{v}, t)$. Here we neglect collective effects [42-44], i.e. by dipole-dipole interaction between active atoms, considering the medium sufficiently rarefied. The equation for the density matrix in the Wigner representation for the translational degrees of freedom of atoms can be written as

$$\dot{\hat{\rho}} + \mathrm{v}\nabla\hat{\rho} = -\frac{i}{\hbar}[\hat{H}, \hat{\rho}] + \hat{\hat{\Gamma}}(\hat{\rho}) + \hat{\hat{S}}(\hat{\rho}), \quad (3)$$

where $\hat{\hat{\Gamma}}$, $\hat{\hat{S}}$ — are superoperators phenomenologically accounting for spontaneous decay of excited states of active atoms and their collisions with buffer gas atoms respectively, υ is the translational velocity vector of atoms $\hbar$, is the reduced Planck constant.

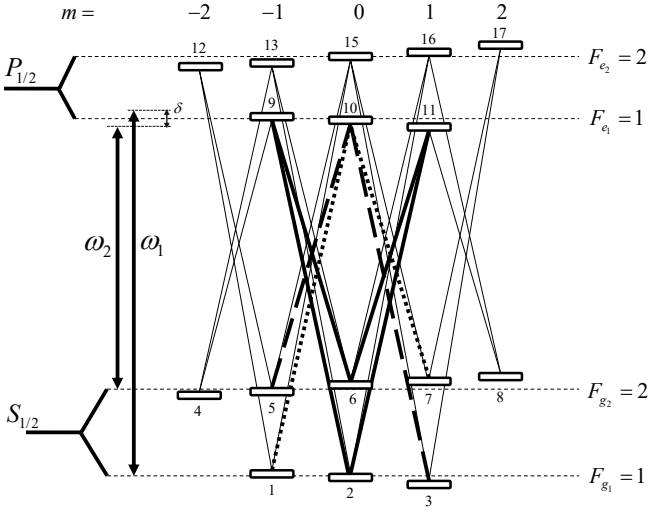

Fig. 1. Pumping scheme of the D_1-line of the atom ^{87}Rb

The system Hamiltonian can be represented as

$$\hat{H} = \hat{H}_0 - \hbar\hat{V}, \tag{4}$$

where

$$\hat{H}_0 = \sum_n \hbar\omega_n^{at} |n\rangle\langle n|$$

— is the free atom Hamiltonian, ω_n^{at} — are the atomic energy level frequencies n ($n = 1,...,16$).

The interaction Hamiltonian $\hat{V}$ is written in the dipole approximation:

$$\hat{V} = \frac{\hat{\mathbf{d}}\cdot\mathbf{E}}{\hbar} = \frac{1}{\hbar}[(\hat{\mathbf{d}}\cdot\mathbf{e}_1)E_1 \exp - i(\omega_1 t - k_1 z) + \\ + (\hat{\mathbf{d}}\cdot\mathbf{e}_2)E_2 \exp - i(\omega_2 t - k_2 z) + \text{H.c.}]. \tag{5}$$

Here $\hat{d}$ — is the dipole moment vector operator. We express it through contravariant cyclic unit vectors:

$$\hat{\mathbf{d}} = \hat{d}^{+}\mathbf{e}^{+} + \hat{d}^{-}\mathbf{e}^{-} + \hat{d}^{0}\mathbf{e}_z. \tag{6}$$

The matrix elements values of cyclic components of the dipole moment operator for optical transitions can be found using the Wigner-Eckart theorem [45] and spontaneous decay theory [46]:

$$d^{q}_{e_j,\,g_j} = (-1)^{Fg_j + J + I - 1}\sqrt{(2J+1)(2F_{g_j}+1)}\times \\ \times C^{F_{e_j},\,m_{e_j},}_{F_{g_j},\,m_{g_j},\,1,\,q}\begin{Bmatrix} I & F_{e_j}, & J \\ 1 & J & Fg_j \end{Bmatrix} V_0, \tag{7}$$

where

$$V_0 = \sqrt{\frac{3\hbar c^3\gamma}{4\omega_{D_1}^3}};$$

γ — is the spontaneous decay rate of the excited state; ω_{D_1} — is the frequency of the unsplit transition of the D_1-line; c — is the speed of light in vacuum; $F_{g_j(e_j)} = 1,2$, $J = 1/2$, $I = 3/2$ — are the absolute values of the total atomic momentum at level $|g_j\rangle(|e_j\rangle)$, electron shell momentum at level $|n\rangle$ and nuclear momentum respectively; m_n — is the projection value of the total momentum at level $|n\rangle$; $C^{F_e,m_e}_{F_g,m_g,1,q}$ — are Clebsch-Gordan coefficients; curly brackets denote $6j$-symbols; $g_1 = 1,...,3$; $g_2 = 4,...,8$; $e_1 = 9,...,11$; $e_2 = 12,...,16$; $q = \pm 1$;

$$\rho_{g_j e} = \rho^{*}_{e g_j} = e^{i(\omega_j t - k_j z)}\tilde{\rho}_{g_j e}, \tag{8}$$

$$\rho_{g_1 g_2} = \rho^{*}_{g_2 g_1} = e^{i[(\omega_1-\omega_2)t - (k_1 - k_2)z]}\tilde{\rho}_{g_1 g_2}. \tag{9}$$

The detunings of fields from corresponding unsplit transitions are defined, assuming tuning to levels with $F_e = 1$, as follows:

$$\Delta_j = \omega_j - \left(\omega_{D_1} + \Delta^{hfs}_{e_1} - \Delta^{hfs}_{g_j}\right), \tag{10}$$

where Δ^{hfs}_n — are the hyperfine splitting frequencies of levels $|n\rangle$.

Taking into account substitutions (8), (9), let's write out element by element equation (3), excluding terms oscillating with double frequency $\left(\propto e^{2i(\omega_j t - k_j z)}\right)$, within the rotating wave approximation:

$$\dot{\rho}_{gg}(\upsilon) + \nabla\rho_{gg}(\upsilon) = \\ = i\sum_{e=9}^{16}\left(\tilde{V}^{*}_{eg}\tilde{\rho}_{eg}(\upsilon) - \tilde{\rho}_{ge}(\upsilon)\tilde{V}_{eg}\right) + \\ + \sum_{e=9}^{16}\gamma_{eg}\rho_{ee}(\upsilon) - \nu\rho_{gg}(\upsilon) + \\ + \sum_{g'=1}^{8}\nu_{g'g}M(\upsilon)\int\rho_{g'g'}(\upsilon')d^{3}\upsilon' + \\ + \sum_{e=9}^{16}\nu_{eg}M(\upsilon)\int\rho_{ee}(\upsilon')d^{3}\upsilon', \tag{11}$$

$$\dot{\rho}_{ee}(\upsilon) + \upsilon\nabla\rho_{ee}(\upsilon) = $$
$$= i\sum_{g=1}^{8}\left(\tilde{V}_{eg}\tilde{\rho}_{ge}(\upsilon) - \tilde{\rho}_{eg}(\upsilon)\tilde{V}^{*}_{eg}\right) -$$
$$-(\gamma + \nu)\rho_{ee}(\upsilon) +$$
$$+\sum_{e'=9}^{16}\nu_{e'e}M(\upsilon)\int\rho_{e'e'}(\upsilon')d^{3}\upsilon', \quad (12)$$

$$\dot{\tilde{\rho}}_{g_j e}(\upsilon) + \upsilon\nabla\tilde{\rho}_{g_j e}(\upsilon) = $$
$$= -i(\Delta_j + \Delta_{g_j e} - \mathbf{k}_j\cdot\upsilon)\tilde{\rho}_{g_j e}(\upsilon) +$$
$$+i\sum_{g'_j}\rho_{g_j g'_j}(\upsilon)\tilde{V}^{*}_{eg'_j} - \left(\frac{\gamma}{2} + \nu\right)\tilde{\rho}_{g_j e}(\upsilon), \quad (13)$$

$$\dot{\tilde{\rho}}_{g_1 g_2}(\upsilon) + \upsilon\nabla\tilde{\rho}_{g_1 g_2}(\upsilon) = $$
$$= i\sum_{e=9}^{16}\left(\tilde{V}^{*}_{eg_1}\tilde{\rho}_{eg_2}(\upsilon) - \tilde{\rho}_{g_1 e}(\upsilon)\tilde{V}_{eg_2}\right) -$$
$$-i(\Delta_1 - \Delta_2 + \Delta_{g_1 g_2} - \mathbf{q}\cdot\upsilon)\tilde{\rho}_{g_1 g_2}(\upsilon) -$$
$$-\nu\tilde{\rho}_{g_1 g_2}(\upsilon) + \nu^{rf}_{S_{1/2}}M(\upsilon)\int\tilde{\rho}_{g_1 g_2}(\upsilon')d^{3}\upsilon', \quad (14)$$

$$\dot{\rho}_{g_j g'_j}(\upsilon) + \upsilon\nabla\rho_{g_j g'_j}(\upsilon) = $$
$$= i\sum_{e=9}^{16}\left(\tilde{V}^{*}_{eg_j}\tilde{\rho}_{eg'_j}(\upsilon) - \tilde{\rho}_{g_j e}(\upsilon)\tilde{V}_{eg'_j}\right) +$$
$$+i\omega_{g_j g'_j}\rho_{g_j g'_j}(\upsilon) - \nu\rho_{g_j g'_j}(\upsilon) +$$
$$+\nu^{zee}_{S_{1/2}}M(\upsilon)\int\rho_{g_j g'_j}(\upsilon')d^{3}\upsilon', \quad g'_j \neq g_j. \quad (15)$$

Here, the following notations are introduced

$$\Delta_{g_j e_i} = \Delta^{hfs}_{e_1} + \Delta^{mag}_{g_j} - (\Delta^{hfs}_{e_i} + \Delta^{mag}_{e_i}),$$

$$\Delta_{g_1 g_2} = \Delta^{mag}_{g_1} - \Delta^{mag}_{g_2},$$

Δ^{mag}_{n} — frequencies of magnetic level splitting $|n\rangle$ (estimated using the Breit-Rabi formula [47] with accuracy up to the quadratic term in magnetic field);

$$M(\upsilon) = \left(\sqrt{\pi}\upsilon_T\right)^{-3}\exp\left(-\upsilon^2 / \upsilon_T^2\right)$$

— Maxwell distribution, υ_T — most probable thermal velocity; γ — decay rates of excited states; $\gamma_e g$ — decay rates of excited levels $|e\rangle$ to levels $|g\rangle$;

$$\tilde{V}_{eg_j} = (d_{eg_j}e_j)E_j / \hbar$$

— generalized Rabi frequencies of corresponding transitions; ν_{nm} — collision frequencies leading to transitions $|n\rangle \to |m\rangle$; ν — total collision frequency; $\nu^{rf}_{S_{1/2}}$, $\nu^{zee}_{S_{1/2}}$ — collision frequencies that do not lead to destruction of radio-frequency and Zeeman coherences between sublevels $S_{1/2}$-states respectively (the latter is assumed equal to in calculations ν); $\omega_{nm} = \omega_m - \omega_n$; $g = 1,...,8$, $e = 9,...,16$. Here, the collision integrals are written in the strong collision model [48], and equations for coherences between excited state sublevels $\tilde{\rho}_{ee'}$ are discarded within the adiabatic approximation ($\tilde{V}_{eg} \ll \nu$). The values of constants for the atom ^{87}Rb are taken from work [47].

Using a model where atomic populations after collisions become uniformly mixed across ground and excited multiplets [48], we relate frequencies ν_{nm} to the total collision frequency ν as follows:

$$\nu_{g'g} = \begin{cases} \nu(1-\eta^{rf}), & g' = g, \\ \dfrac{\eta^{rf}\nu}{N_{S_{1/2}} - 1}, & g' \neq g, \end{cases}$$
$$\nu_{e'e} = \begin{cases} \nu\left(1 - \eta'^{rf} - \eta^{opt}\right), & e' = e, \\ \dfrac{\eta'^{rf}\nu}{N_{P_{1/2}} - 1}, -\eta^{opt}), & e' \neq e, \end{cases} \quad (16)$$

where $N_{S_{1/2}} = N_{P_{1/2}} = 8$ — numbers of sublevels $S_{1/2}$- and $P_{1/2}$-states, respectively; η^{rf}, η'^{rf} — fractions of collisions leading to population mixing between ground and excited state sublevels respectively; η^{opt} — fraction of collisions leading to excitation quenching. The value ν can be estimated from the gas-kinetic formula $\nu = (n_a + n_{buf})\sigma\bar{u}$, where n_a — concentration of active atoms, n_{buf} — buffer gas concentration, σ — cross-section of the corresponding process, $\bar{u} = \sqrt{8kT / \pi\mu}$ — mean thermal velocity, μ — reduced mass of active atom and buffer gas atom. Note that the buffer gas atom concentration n_{buf} in the ensemble is much higher than the concentration of active atoms n_a. Due to this, the temperature dependence of frequency ν can be neglected, as only concentration n_a depends on the latter.

We will limit ourselves to the approximations of a plane wave front, small diffraction of the field at the medium edges, and uniformity of its

optical properties. Furthermore, we will neglect diffusion effects, assuming that the diffusion length during excitation time τ_e is much smaller than the characteristic dimensions of the medium L: $\sqrt{D\tau_e} \ll L$, where D — is the diffusion coefficient. All this allows us to neglect the dependence of the density matrix on coordinates in directions transverse to the laser beam $\hat{\rho} = \hat{\rho}(,z,t)$.

We will transition to the reduced density matrix

$$\overline{\rho}_{nm}(z,t) = \int \rho_{nm}(\upsilon,z,t)d^3\upsilon$$

the symbol <<∼>> above the letter for cases $n \neq m$ is omitted) by integrating the equations over velocities. Using the weak field approximation, the velocity dependencies of ground state populations $\rho_{gg}(\upsilon)$ and coherences between magnetic $\rho_{g_jg'_j}(\upsilon)$ and hyperfine $\rho_{g_1g_2}(\upsilon)$ sublevels of the ground state can be approximately considered Maxwellian [29]:

$$\rho_{gg'}(\upsilon,z,t) = M(\upsilon)\overline{\rho}_{gg'}(z,t). \qquad (17)$$

This approximation is due to the assumed narrow laser line compared to the Doppler width, small Rabi frequencies compared to γ and long coherence lifetime between ground state sublevels. As a result of integration for equations (11), (12), (14), (15), we obtain

$$\dot{\overline{\rho}}_{g_jg_j} = i\sum_{e=9}^{16}\left(\tilde{V}^*_{eg_j}\overline{\rho}_{eg_j} - \overline{\rho}_{g_je}\tilde{V}_{eg_j}\right) + \frac{\gamma'}{N_{S_{1/2}}}\overline{\rho}_{exc} - \eta^{rf}\nu\overline{\rho}_{g_jg_j} + \frac{\eta^{rf}\nu}{N_{S_{1/2}}-1}\sum_{\substack{g'=1\\ g'\neq g}}^{8}\overline{\rho}_{g'g'}, \qquad (18)$$

$$\dot{\overline{\rho}}_{exc} = i\sum_{e=9}^{16}\sum_{g=1}^{8}\left(\tilde{V}_{eg}\overline{\rho}_{ge} - \overline{\rho}_{eg}\tilde{V}^*_{eg}\right) - \gamma'\overline{\rho}_{exc}, \qquad (19)$$

$$\dot{\overline{\rho}}_{g_1g_2} = i\sum_{e=9}^{16}\left(\tilde{V}^*_{eg_1}\overline{\rho}_{eg_2} - \overline{\rho}_{g_1e}\tilde{V}_{eg_2}\right) - (i(\Delta_1 - \Delta_2 + \Delta_{g_1g_2}) + \gamma_{12})\overline{\rho}_{g_1g_2}, \qquad (20)$$

$$\dot{\overline{\rho}}_{g_jg'_j} = i\sum_{e=9}^{16}\left(\tilde{V}^*_{eg_j}\overline{\rho}_{eg'_j} - \overline{\rho}_{g_je}\tilde{V}_{eg'_j}\right) + i\omega_{g_jg'_j}\overline{\rho}_{g_jg'_j}, \qquad (21)$$

where

$$\overline{\rho}_{exc} = \sum_e \overline{\rho}_{ee}$$

— is the total population of excited states; $\gamma' = \gamma + \nu\eta^{opt}$ — is the collision-modified decay rate of excited states; $\gamma_{12} = \nu - \nu^{rf}_{S_{1/2}}$ — is the collision decay rate of radio-frequency coherences between hyperfine sublevels of the ground state. When obtaining these equations, terms with gradients in the left parts of equations (11), (12), (14), (15), as well as the term in (14) accounting for residual Doppler shift $q\upsilon$, vanish due to approximation (17). Here, when obtaining equation (18), we limited ourselves to considering the case of complete collisional depolarization of the excited state, assuming $\eta'^{rf}\nu \gg \gamma'$, which occurs at relatively high buffer gas pressures [37, 49, 50]. Note that for such pressures, the collisional line broadening becomes comparable to the frequency of hyperfine splitting of the excited state.

In equation (13), the transition to reduced density matrix elements through velocity integration is analytically impossible due to the presence of Doppler terms proportional to $\mathbf{k}_j \cdot \upsilon$. Therefore, we first express optical coherences through quadratures and then integrate over velocities:

$$\overline{\rho}_{g_je_i}(t) = i\int_0^t dt'\sum_{g'_j}\overline{\rho}_{g_jg'_j}(t')\tilde{V}^*_{e_ig'_j}(t') \times \int d^3\upsilon M(\upsilon) \times \exp[-(i(\Delta_j + \Delta_{g_je_i} - \mathbf{k}_j\cdot\upsilon) + \Gamma')(t-t')], \qquad (22)$$

where

$$\Gamma' = \gamma/2 + \nu.$$

Performing velocity integration in (22), we obtain

$$\overline{\rho}_{g_je_i}(t) = i\int_0^t dt' \times \exp\left[-\frac{\upsilon_T^2\mathbf{k}_j^2}{4}(t-t')^2 - (i\Delta_j + i\Delta_{g_je_i} + \Gamma')(t-t')\right] \times \sum_{g'_j}\overline{\rho}_{g_jg'_j}(t')\tilde{V}^*_{e_ig'_j}(t'). \qquad (23)$$

By substituting (23) into (18)-(21), we obtain a system of Volterra integro-differential equations of the second kind, which allows further numerical solution.

3. RESULTS

This work investigates CPT resonances detected by two rectangular pulses separated in time by a dark pause (Fig. 2). The duration of the first pumping

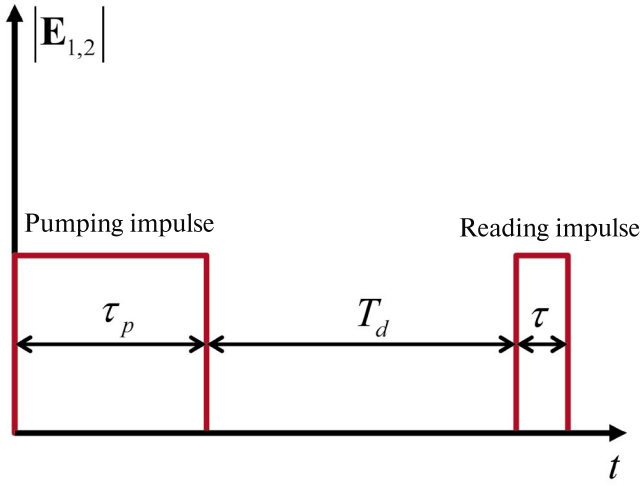

Fig. 2. Sequence of pumping pulses

pulse is assumed to be much longer than the time required to establish a steady-state CPT, which allows using the stationary solution of system (18)-(21) at the end of the pumping pulse. The duration of the dark pause is assumed to be much longer than the decay times of all optical coherences and excited state populations.

By calculating the dependence of the total excited state population on the two-photon detuning $\overline{\rho}_{exc}(\delta)$ at the end of the readout pulse, we obtain the spectrum of CPT resonances detected by the Ramsey method. For convenience of analysis, we will consider the resonance contrast, which we define as follows:

$$C(\delta) = 1 - \frac{\overline{\rho}_{exc}(\delta)}{\overline{\rho}_{exc}(\delta_{off})},$$

where δ_{off} — is the value of two-photon detuning outside the CPT resonance.

Let's analyze the influence of the magnetic field on the CPT-Ramsey resonance spectrum and do this for two known polarization field configurations *lin* ⊥ *lin* [51] and *lin* ∥ *lin* [52]. Fig. 3 shows that the amplitude of Ramsey resonances is lower than the amplitude of resonances detected by continuous radiation. This is explained by the decay of low-frequency coherences between the sublevels of the ground state during the dark pause. Thus, increasing the duration of the dark pause leads, on the one hand, to narrowing of resonances, but on the other hand, to a decrease in their amplitude. Increasing the magnetic field allows to distinguish individual maxima of the envelope in the Ramsey comb,

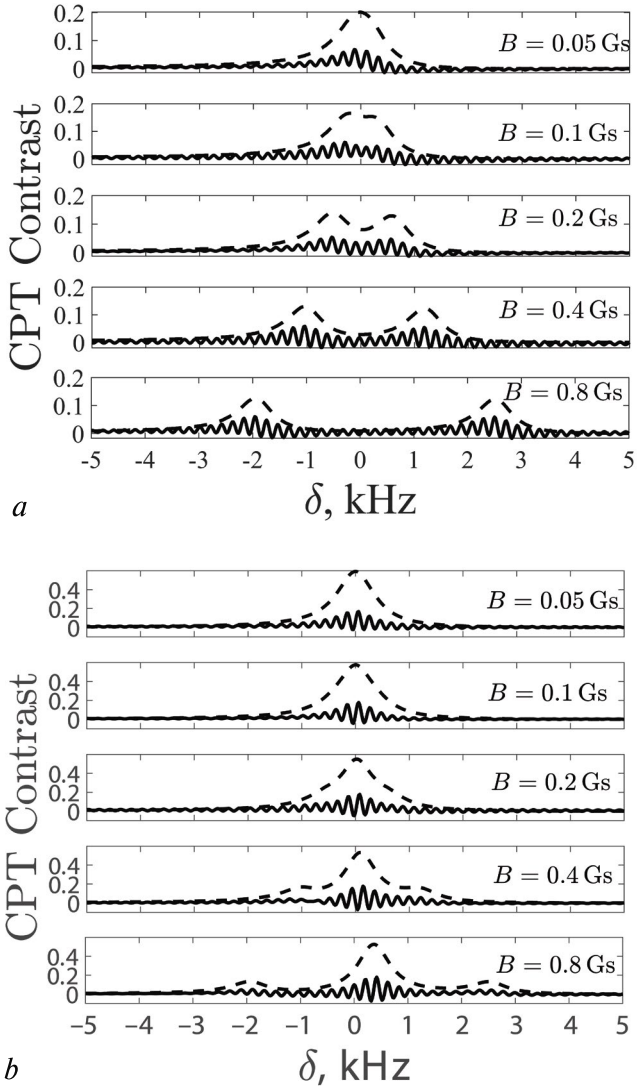

Fig. 3. Magnetic field dependencies of contrast CPT resonance spectra detected using the Ramsey method (solid curves) and continuous radiation (dashed curves), for configurations *lin* ⊥ *lin* (*a*) and *lin* ∥ *lin* (*b*). Calculation parameters: $I_1 = I_2 = 0.2\text{mW/cm}^2$, $T = 40\,^{\circ}\text{C}$, $T_d = 5$ ms, $\gamma_{12} = 250\ \text{s}^{-1}$, $\eta^{opt} = 0.2$, $\eta^{rf} = 2\gamma_{12} / v$, $n_{buf} = 4 \cdot 10^{18}\,\text{cm}^{-1}$, buffer gas — nitrogen

corresponding to CPT resonances at radiofrequency transitions $|1\rangle \leftrightarrow |7\rangle$, $|2\rangle \leftrightarrow |6\rangle$ and $|3\rangle \leftrightarrow |5\rangle$, whose positions are given by the differences in magnetic shifts of the corresponding transitions: Δ_{71}, Δ_{62} and Δ_{53}. At the same time, the resonance at the radio-frequency transition $|2\rangle \leftrightarrow |6\rangle$, (bold lines in Fig.1) is absent for the *lin* ∥ *lin* configuration, due to destructive interference of two lambda schemes at this transition, as shown in [53].

Let's analyze the change in the shape of Ramsey resonances with increasing magnetic field in more

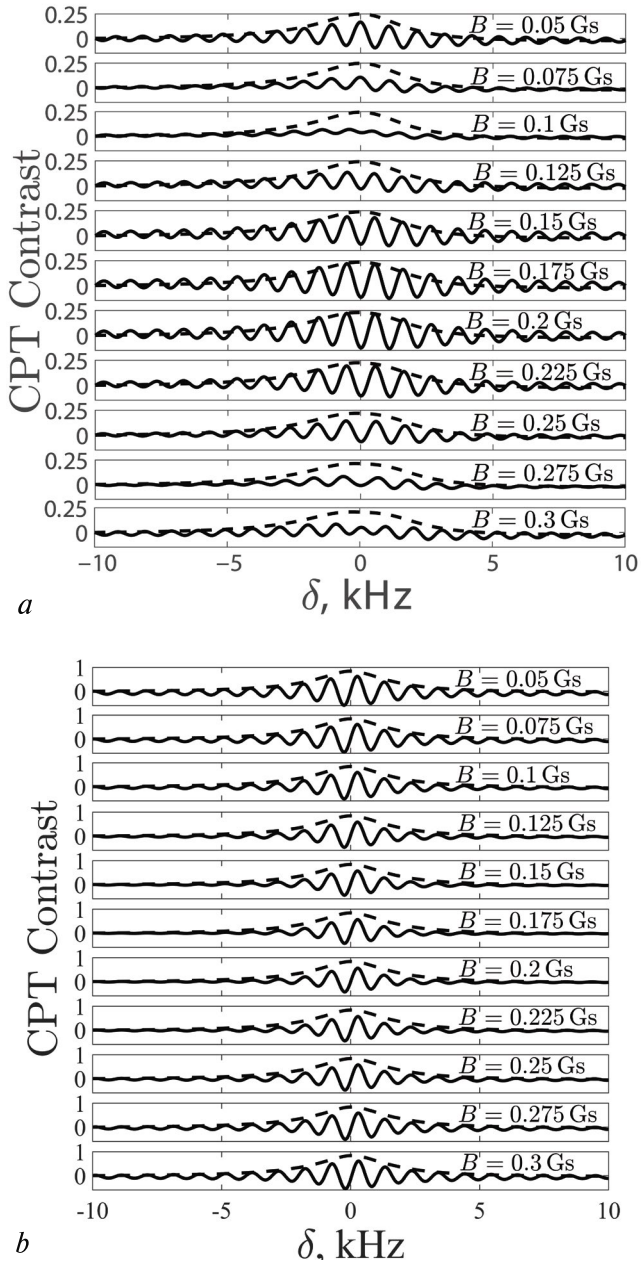

Fig. 4. Magnetic field dependencies of contrast CPT resonance spectra detected using the Ramsey method (solid curves) and continuous radiation (dashed curves), for configurations *lin* ∥ *lin* (*a*) and *lin* ⊥ *lin* (*b*). Calculation parameters: $I_1 = I_2 = 1\text{mW/cm}^2$, $T = 40^\circ$ C, $T_d = 1$ ms. Other parameters are the same as in the caption to Fig. 3

detail. Figure 4 demonstrates a non-monotonic dependence of Ramsey resonance amplitude on magnetic field. In particular, at certain magnetic field values, the resonance amplitude reaches a local minimum. This result is consistent with experimental data [54] and is explained by destructive interference of different excitation channels of Ramsey CPT resonances. During the dark pause, low-frequency coherences $\bar{\rho}_{g_1g_2}$ change phase by $(\delta + \Delta_{g_1g_2})T_d$. If by the end of the dark pause different coherences of two working sublevels g_1g_2 and $g_1'g_2'$ are in antiphase, i.e., the condition

$$\left(\Delta_{g_1g_2} - \Delta_{g_1'g_2'}\right)T_d = \pi(2p-1), \quad p = 1,2,..., \quad (24)$$

is met, then the corresponding lambda schemes will weaken each other. Thus, using expression (24), we obtain that at $T_d = 1$ ms, lambda schemes at transitions $|1\rangle \leftrightarrow |7\rangle$ and $|3\rangle \leftrightarrow |5\rangle$ will weaken each other for $B \approx 0.09, 0.27, 0.45, ...$G, which is clearly visible in Fig. 4*a*, since for configurations *lin* ∥ *lin* resonance at transition $|2\rangle \leftrightarrow |6\rangle$ is absent. It is noteworthy that in this case, when passing through these magnetic field values, the central peak changes its convexity. In configuration *lin* ⊥ *lin* the main contribution to the attenuation of the Ramsey comb amplitude is jointly made by interference between lambda schemes at radiofrequency transitions $|1\rangle \leftrightarrow |7\rangle$ and $|2\rangle \leftrightarrow |6\rangle$, as well as $|2\rangle \leftrightarrow |6\rangle$ and $|3\rangle \leftrightarrow |5\rangle$. Thus, from (24) we obtain that at $T_\text{d} = 1$ ms, the minimum amplitude is first reached in the interval $B \in 0.09–0.18$. However, due to the fact that the resonance at transition $|2\rangle \leftrightarrow |6\rangle$ has a significantly larger amplitude, the interference contribution of adjacent resonances in this case turns out to be small, and in Fig. 4*b* the amplitude changes extremely weakly. Thus, the amplitude of Ramsey resonances for *lin* ⊥ *lin* configuration is less sensitive to magnetic field changes. Note that formula (24) neglects the influence of light shift.

Fig. 5 shows how the Ramsey comb changes during the transition from *lin* ⊥ *lin* configuration to right circular polarization of both fields. It can be seen that in the envelope of the Ramsey comb, with increasing ellipticity, only one minimum remains, corresponding to the resonance at transition $|2\rangle \leftrightarrow |6\rangle$. The amplitude of resonances decreases due to the formation of a "pocket" at the level, which makes the use of circular polarization in CPT excitation less advantageous. From Fig. 5*a*,*b* it can be seen that this occurs both for short $T_\text{d} = 1$, and long $T_\text{d} = 5$ dark pause.

In Fig. 6*a* comparison of Ramsey resonances behavior when increasing ellipticity for configurations $\sigma^+\sigma^+$ and $\sigma^+\sigma^-$ with initial *lin* ∥ *lin* configuration is presented. It can be seen that

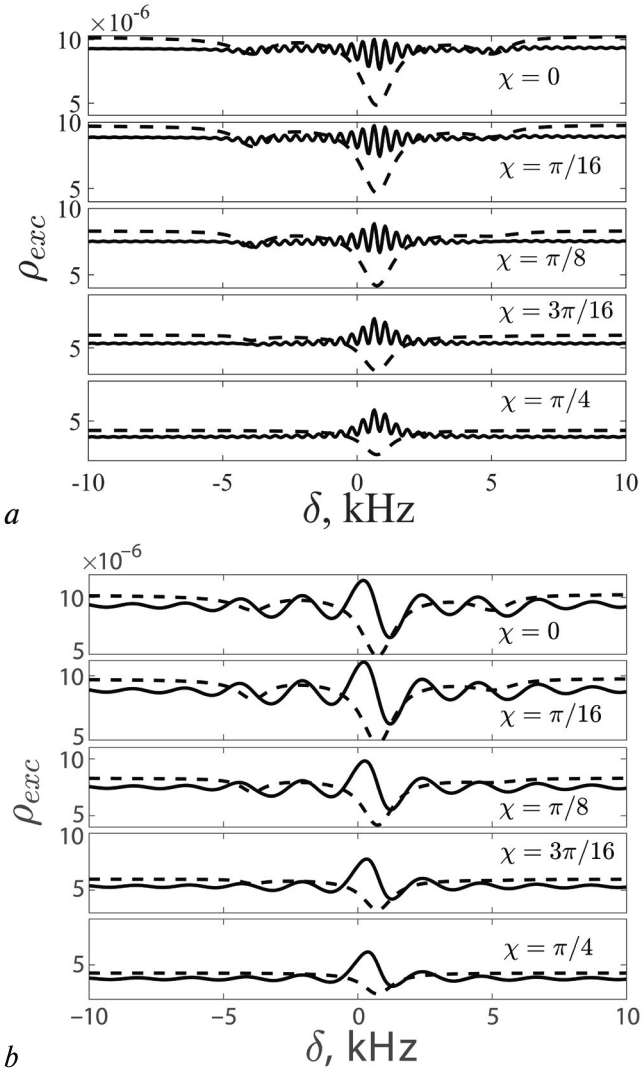

Fig. 5. Dependencies of CPT resonance spectra detected by Ramsey method (solid curves) and continuous radiation (dashed curves) on ellipticity parameter χ during transition from configuration *lin* ⊥ *lin* to right circular polarization of both fields for T_d = 5 ms (*a*), 1 ms (*b*). Calculation parameters: $I_1 = I_2 = 0.2$ ìmW/cm^2 , $T = 40^\circ$ C, $B = 0.8$ G . Other parameters are the same as in caption to Fig. 3

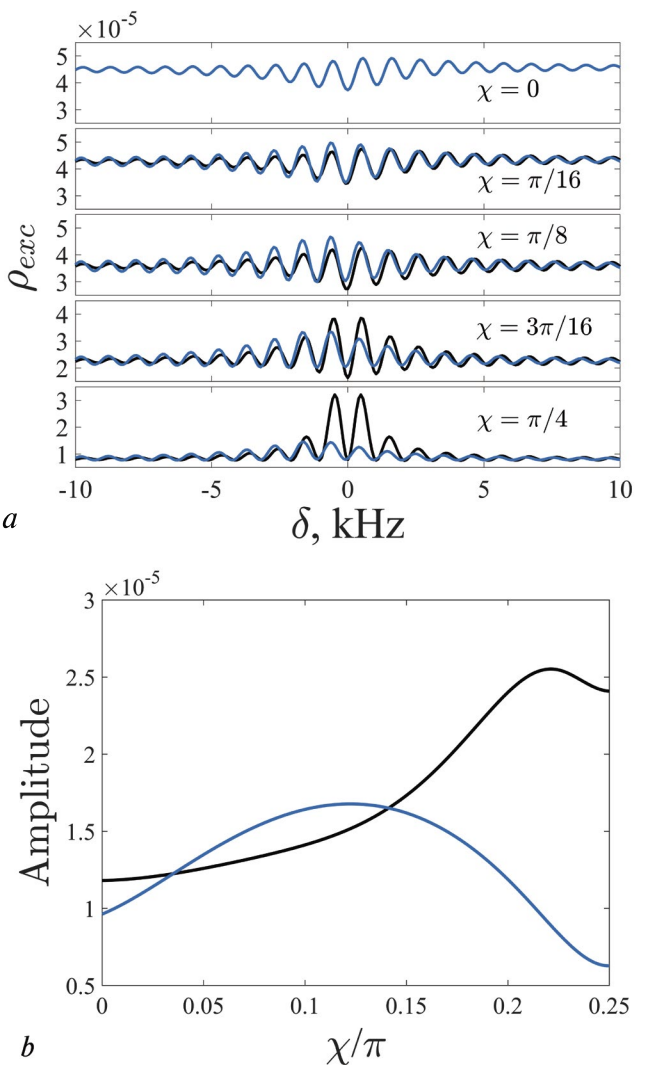

Fig. 6. Dependencies of spectra (a) and amplitudes (b) of CPT resonances detected by Ramsey method on ellipticity parameter of two right-circularly polarized waves ($\sigma^+\sigma^+$) (blue curve) and one right- and another left-circularly polarized waves ($\sigma^+\sigma^-$) (black curve) at configuration *lin* ∥ *lin* for $\chi = 0$. Calculation parameters: $I_1 = I_2 = 1$ mW/cm^2, $T = 40^\circ$C, $T_d = 1$ ms, $B = 0.05$ G. Other parameters are the same as in caption to Fig. 3

during the transition to circular polarizations, a peak remains in the resonance envelope, in the case of $\sigma^+\sigma^-$ corresponding to the CPT resonance at the transition $|2\rangle \leftrightarrow |6\rangle$, and in the case of $\sigma^+\sigma^+$ — at the transition $|1\rangle \leftrightarrow |7\rangle$. Note that the position of the latter differs somewhat from the value Δ_{71}, due to the light shift influence. The amplitude of the central resonance envelope extremum changes non-monotonically with ellipticity change, having a pronounced maximum in the vicinity of π / 8 for the configuration case $\sigma^+\sigma^-$ (Fig. 6b). Thus, for configuration $\sigma^+\sigma^-$ there exists an optimal ellipticity where the resonance has the best quality parameter. This effect can also be explained by the interference influence of different Λ-schemes. As noted above, in *lin* ∥ *lin* configuration, the resonance at radio frequency transition $|2\rangle \leftrightarrow |6\rangle$ absent. During transition to circular polarization $\sigma^+\sigma^+$ only one of its legs is observed due to selection rules. However, at intermediate ellipticity values between *lin* ∥ *lin*- and $\sigma^+\sigma^+$-polarizations, the second leg of the double Λ-scheme at transition $|2\rangle \leftrightarrow |6\rangle$ manifests itself, making a constructive contribution to the spectrum at small values of magnetic field. It should be noted that at magnetic field values satisfying the

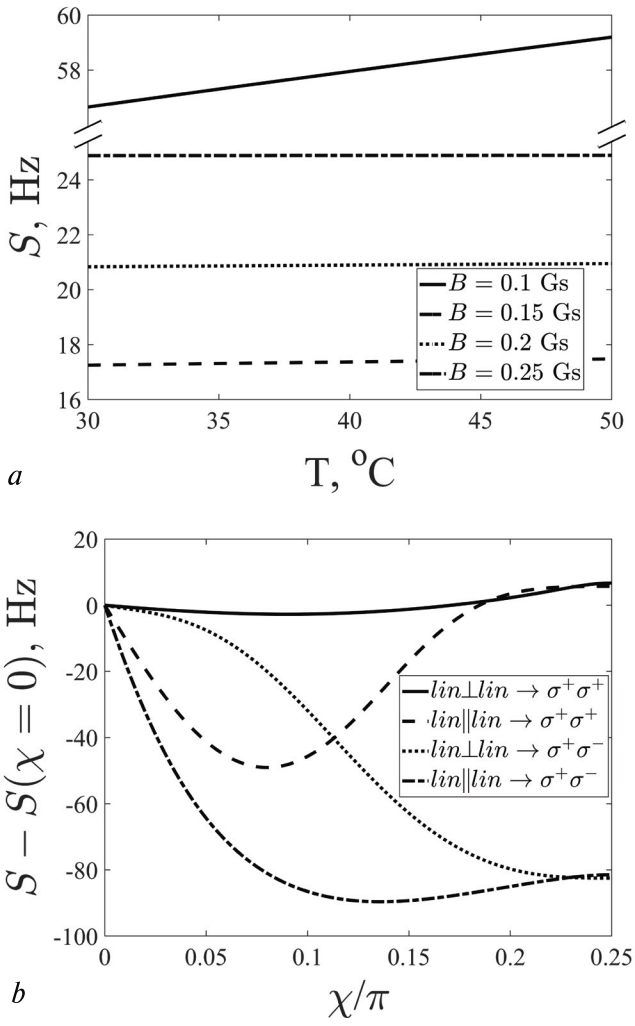

Fig. 7. Dependencies of the CPT central resonance shift S, detected by the Ramsey method, on temperature at different magnetic field values B for configuration *lin* ∥ *lin* (*a*) and on ellipticity during transition to different circular polarization configurations (*b*). Calculation parameters: $I_1 = I_2 = 1\,\text{mW/cm}^2$, $T = 40^\circ$ C, $T_d = 1$ ms. Other parameters are the same as in the caption to Fig. 3

destructive interference condition (24), ellipticity change will lead to the opposite effect.

Let's analyze the behavior of the light shift of the central Ramsey resonance. From Fig. 7*a* it can be seen that the temperature dependence of the shift in the specified range is close to linear, which agrees with the results of work [29], where such behavior was explained by temperature broadening of the dispersion contour. The change in the magnetic field leads to a change in the slope angle of the dependence, due to Zeeman shifts of working sublevels. Thus, by choosing the magnetic field magnitude, it becomes possible to suppress the temperature dependence of the shift. In Fig. *b* the dependencies of the relative shift of the central Ramsey resonance on the degree of field ellipticity during transition from linear polarizations to circular ones are presented. It can be seen that the course of these dependencies becomes more gentle in the vicinity of $\pi / 4$, which is explained by the isotropy of the system in the plane transverse to the laser beam. Thus, resonances excited by circularly polarized fields prove to be less sensitive to ellipticity fluctuations compared to resonances excited by linearly polarized fields, both in amplitude (Fig. 6*b*) and in shift (Fig. 7*b*).

4. CONCLUSION

In this work, based on the density matrix method in the Wigner representation for translational degrees of freedom of atoms, a theory of excitation of coherent population trapping resonances detected by the Ramsey pulse excitation method in gas cells with vapors ^{87}Rb has been developed. The constructed theory takes into account the complete magnetic structure of levels of the D_1-line ^{87}Rb and can be used in the analysis of other non-stationary effects arising from the interaction of resonant bichromatic radiation with atomic vapors ^{87}Rb. The spectra of CPT-Ramsey resonances have been calculated, and the dependence of their shape and shifts on various pumping parameters, such as external magnetic field magnitude, ellipticity degree of frequency radiation components, and medium temperature, has been studied. It was established that there is interference between different channels of Ramsey resonance excitation, manifesting as a non-monotonic change in resonance amplitude depending on the magnetic field magnitude. Expressions are proposed for estimating parameter regions that realize destructive interference, leading to minimal resonance amplitudes. The existence of optimal resonance amplitude ellipticity of external fields was discovered when using the $\sigma^+\sigma^-$-configuration. When analyzing resonance shifts, the possibility of suppressing the dependence of these shifts on temperature and ellipticity was demonstrated through selection of specific magnetic field values and polarizations, respectively.

FUNDING

This work was financially supported by the Russian Science Foundation, grant No. 21-72-10004 (development of numerical

algorithms for solving systems of integro-differential equations). G. V. Voloshin thanks the Theoretical Physics and Mathematics Advancement Foundation "BASIS" for supporting the research conducted within this work on the features of ensemble temperature influence and related atomic motion on collective effects due to finite optical thickness (grant No. 21-1-1-36-1), and the project supervisor I. M. Sokolov.

REFERENCES

1. 1G. Alzetta et al., Nuovo Cim. B 36, 5 (1976).

2. E. Arimondo and G. Orriols, Lett. Nuovo Cim. 17, 333 (1976).

3. H. R. Gray, R. M. Whitley, and C. R. Stroud, Jr., Opt. Lett. 3, 218 (1978).

4. B. D. Agapiev, M. B. Gornyi, B. G. Matisov et al., UFN 163, 1 (1993).

5. A. Akulshin, A. Celikov, and V. Velichansky, Opt. Commun. 84, 139 (1991).

6. P. D. D. Schwindt, S. Knappe, V. Shah, L. Hollberg, and J. Kitching, Appl. Phys. Lett. 85, 6409 (2004).

7. R. Mhaskar, S. Knappe, and J. Kitching, A LowPower, High-Sensitivity Micromachined Optical Magnetometer, Appl. Phys. Lett. 101, 241105 (2012).

8. V. Andryushkov, D. Radnatarov, and S. Kobtsev, Appl. Opt. 61, 3604 (2022).

9. O. Kocharovskaya and Ya.I. Khanin, JETP Lett. 48, 581 (1988).

10. M. D. Lukin, Rev. Mod. Phys. 75, 457 (2003).

11. M. Fleischhauer, A. Imamoglu, and J. P. Marangos, Rev. Mod. Phys. 77, 633 (2005).

12. R. Zhang and X.-B. Wang, Phys. Rev. A 94, 063856 (2016).

13. J. Vanier, Appl. Phys. B 81, 421 (2005).

14. S. A. Zibrov, V. L. Velichansky, A. S. Zibrov et al., JETP Lett. 82, 534 (2005).

15. S. A. Zibrov, I. Novikova, D. F. Phillips et al., Phys. Rev. A 81, 013833 (2010).

16. J. Kitching, Chip-Scale Atomic Devices, Appl.Phys. Rev. 5, 031302 (2018).

17. S. Kobtsev, S. Donchenko, S. Khripunov, D. Radnatarov, I. Blinov, and V. Palchikov, Opt. Laser Technol. 119, 105634 (2019).

18. M. N. Skvortsov, S. M. Ignatovich, V. I. Vishnyakov et al., Quantum Electronics 50, 576 (2020).

19. M. Petersen, M. A. Hafiz, E. de Clercq, and Ro. Boudot, JOSA B 39, 910 (2022).

20. G. D. Martinez, C. Li, A. Staron et al., Nat. Commun. 14, 3501 (2023).

21. N. F. Ramsey, Phys. Rev. 76, 996 (1949).

22. F. Rihle, Frequency Standards: Principles and Applications, Fizmatlit, Moscow (2009).

23. M. Gozzelino, S. Micalizio, F. Levi, A. Godone, and C. E. Calosso, IEEE Trans. on Ultrasonics, Ferroelectrics, and Frequency Control 65 (2018).

24. S. Micalizio and A. Godone, Phys. Rev. A 99, 043425 (2019).

25. K. A. Barantsev, E. N. Popov, A. N. Litvinov, Quantum Electronics 7, 615 (2018).

26. V. N. Baryshev, G. V. Osipenko, M. S. Aleynikov, I. Yu. Blinov, Quantum Electronics 49, 283 (2019).

27. P.-F. Cheng, J.-W. Zhang, and L.-J. Wang, Chinese Phys. B 28, 070601 (2019).

28. G. V. Voloshin, K. A. Barantsev, E. N. Popov, A. N. Litvinov, JETP 156, 5 (2019).

29. G. V. Voloshin, K. A. Barantsev, A. N. Litvinov, Quantum Electronics 50, 1023 (2020).

30. G. V. Voloshin, K. A. Barantsev, A. N. Litvinov, Quantum Electronics 52, 108 (2022).

31. M. A. Hafiz, C. Carlé, N. Passilly, J. M. Danet, C. E. Calosso, and R. Boudot, Appl. Phys. Lett. 120, 064101 (2022).

32. K. A. Barantsev and A. N. Litvinov, JOSA B 39, 230 (2022).

33. D. V. Kovalenko, M. Yu. Basalaev, V. I. Yudin, T. Zanon-Williet, A. V. Taichenachev, KE 51, 495 (2021).

34. V. N. Baryshev, G. V. Osipenko, A. V. Novoselov, A. G. Sukhoverskaya et al., KE 52, 538 (2022).

35. M. Gozzelino, S. Micalizio, C. E. Calosso et al., arXiv: 2308.15249v1 [physics.atom-ph].

36. R. Fang, C. Han, B. J. Lu, and C. Lee, arXiv: 2303.07118v1 [physics.atom-ph].

37. A.V. Taichenachev, V. I. Yudin, R. Wynands, M. Stahler, J. Kitching, and L. Hollberg, Phys. Rev. A 67, 033810 (2003).

38. D.V. Kupriyanov, I. M. Sokolov, N.V. Larionov, P. Kulatunga, C.I. Sukenik, S. Balik, and M. D. Havey, Phys. Rev. A 69, 033801 (2004).

39. V. M. Datsyuk, I. M. Sokolov, D. V. Kupriyanov, and M. D. Havey, Phys. Rev. A 74, 043812 (2006).

40. V. M. Datsyuk, I. M. Sokolov, D. V. Kupriyanov, and M. D. Havey, Phys. Rev. A 77, 033823 (2008).

41. A. S. Kuraptsev, I. M. Sokolov, and M. D. Havey, Phys. Rev. A 96, 023830 (2017).

42. Ya. A. Fofanov, A. S. Kuraptsev, I. M. Sokolov, and M. D. Havey, Phys. Rev. A 84, 053811 (2011).

43. A. S. Kuraptsev and I. M. Sokolov, Phys. Rev. A 90, 012511 (2014).

44. Y. A. Fofanov, I. M. Sokolov, R. Kaiser, and W. Guerin, Phys. Rev. A 104, 02370 (2021).

45. D. A. Varshalovich, A. N. Moskalev, V. K. Khersonskii, Quantum Theory of Angular Momentum, Nauka, Leningrad (1975).

46. V. Weisskopf, Naturwissenschaften 23, 631 (1935).

47. S. G. Rautian, G. I. Smirnov, A. M. Shalagin, Nonlinear Resonances in Atomic and Molecular Spectra, Nauka, Novosibirsk (1979).

48. D. A. Steck, Rubidium 87 D Line Data, http:// steck.us/alkalidata (revision 2.2.1, 21 November 2019).

49. W. Happer, Rev. Mod. Phys. 44, 169 (1972).

50. K. M. Sabakar, M. I. Vaskovskaya, D. S. Chuchelov, E. A. Tsygankov, V.V. Vassiliev, S. A. Zibrov, and V. L. Velichansky, Phys. Rev. Appl. 20, 034015 (2023).

51. T. Zanon, S. Guerandel, E. de Clercq, D. Holleville, N. Dimarcq, and A. Clairon, Phys. Rev. Lett. 94, 193002 (2005).

52. A. V. Taichenachev, V.I. Yudin, V.L. Velichansky, and S. A. Zibrov, JETP Lett. 82, 449 (2005).

53. G. A. Kazakov, B. G. Matisov, I. E. Mazets, Yu. V. Rozhdestvensky, JTP 77, 20 (2006).

54. X. L. Sun, J. W. Zhang, P. F. Cheng, C. Xu, L. Zhao, and L. J. Wang, Opt. Express 24, 4532 (2016).